5 Crystal Engineering

Abstract. In this chapter definitions and methods are given to analyse phase diagrams of different complex compounds from the material science viewpoint with several examples of well known scintillation materials. It is followed by a description of different technologies and equipments for the growth of single crystals. A special attention is paid to the control of parameters, which are particularly important to satisfy some of the user's requirements, like dimensions and homogeneity of optical properties, purity of the initial material and activator uniformity distribution, stoichiometric composition and minimum concentration of point and linear defects. Different techniques to grow single crystalline scintillation materials such as Bridgeman, Stockbarger, Stoeber, Kyropolos, Czochralski as well as state of the art and modern trends in the industrial production are reviewed. Different ways to design the scintillation detector block in such a way to as to maximize the collection efficiency of the scintillation photons are also discussed.

5.1 Phase Diagrams

A large variety of inorganic compounds have the potential to be a scintillator. Crystal chemistry shows a lot of opportunities when systems with two, three, four, and more components are stable because of the strict laws of chemical and crystallography structure formations. In spite of the fact that the development of new crystalline scintillating materials is to a large extent driven by luminescence research another very important part of the study which requires even more efforts is related to the synthesis of a predetermined material if it is at all possible. An initial step is the study of a phase diagram to define the conditions in which a given composition occurs.

The theory of phase diagrams is described elsewhere [1]. This chapter will consider the phase diagrams from the material science point of view and gives examples for some scintillation materials.

The theory of phase balance is based on thermodynamics and establishes relationships between composition, temperature, and pressure in equilibrium systems.

To predict the phase composition of a compound it is necessary to know the number of phases and the number of independent chemical components, from which these phases are formed. The homogeneous part of a

heterogeneous system is called a phase, and the substances forming phases of the chemical system are called chemical components.

For heterogeneous systems the direction of the reactions is determined by the phase rule. According to this rule, the number of degrees of freedom C in an heterogeneous system in equilibrium is equal to the number of independent components $K + 2$, minus the number of phases F: $C = K + 2 - F$. To predict the behavior of the system with the help of the phase rule it is therefore necessary to know the number of phases and the number of independent chemical components. The number of degrees of freedom is defined by thermodynamic parameters (temperature, pressure, composition), which can be modified without changing the number of coexisting phases. If this number is equal to 0, it is impossible to change either the pressure or the composition and temperature without removing one of the phases. The equilibrium at $C = 0$ is called an invariable one. Equilibrium at $C = 1$ is called a mono-variable one for which a given temperature corresponds to a precise value of the vapor pressure. At such a balance it is enough to set up one parameter only, for example a given temperature is sufficient to set the equilibrium pressure and the composition of phases. Equilibrium at $C = 2$ is called bi-variant and it means that an undefined equilibrium pressure corresponds to the given temperature. So, the composition of phases depends both on temperature and on pressure. Constant temperature does not provide, in this case, a constant composition. This conclusion is of great importance in manufacturing crystals, including scintillation materials.

In the case of the phase equilibrium it is convenient to use phase diagrams. For an unicomponent two-phase system the relationship between temperature T and pressure P can be represented on a 2D diagram. In a two-component system the A–B composition is represented by a three-dimensional diagram. For multicomponent systems the representation is multidimensional and it is graphically possible to present only special cases (cross-sections) of multivariable diagrams.

We will analyze here the most common diagrams: "composition – temperature" for binary systems. Such diagrams are most frequently investigated and represent the greatest practical interest for crystal growth from melt.

5.1.1 Phase Diagram of Continuous Solid Solutions

If the chemical components A and B have similar electronic shells structure, ionic radius, or energies of the chemical bonds, they are likely to form a solid solution (see Fig. 5.1). In this case the liquid phase of the composition lies above a liquidus line (L). The solid solution area lies below the solidus line (S). The area of crystallization lies between the solidus and the liquidus curve.

While cooling the melt with composition X (see Fig. 5.1), crystallization will begin at the temperature corresponding to point L_1 on the liquidus curve. The composition of the crystallized solid phase at this time corresponds to

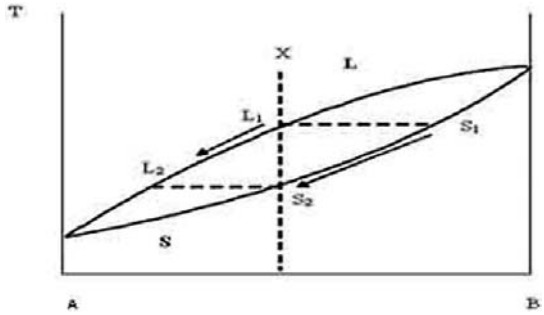

Fig. 5.1. The phase diagram of a binary system with creation of continuous solid solutions

point S_1 on the solidus curve. During further cooling the composition of the crystallized mass will vary along the line S_1–S_2, and the composition of the melt will follow the line L_1–L_2. Thus, the ratio between crystal and melt composition is determined by the line lengths L_2–S_2 and L_1–S_1. If the cooling is very slow the crystal composition will follow the line S^1–S^2. If on the other hand the cooling is fast, a mechanical mixture of crystals having different compositions is formed. This fact is of a very big practical importance for crystallization procedure development.

5.1.2 Eutectic and Distectic Phase Diagram Without Solid Solutions

The diagram for a two-component system A–B is represented schematically in Fig. 5.2. This diagram has two maxima corresponding components' A and B, and a minimum corresponding the eutectic point E.

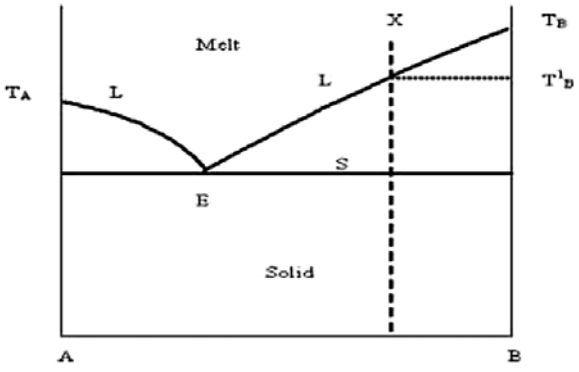

Fig. 5.2. The eutectic phase diagram of a binary system without creation of a compound

This diagram has three domains: the melt area at high temperature, limited by the liquidus curve (L); the area of solid phases at low temperature limited by the solidus horizontal line; and the region of mixed liquid and solid in between.

The crystallization begins when the melt is cooled down to the temperature T_B^1. Further temperature decrease displaces the composition toward the eutectic point E where the solidus and liquidus lines meet. At the eutectic temperature the melt is completely crystallized forming a mechanical mixture of the A and B phases. The eutectic diagram shows that components, A and B coexist but do not react chemically, and that the melting temperature of the pure components decreases to the eutectic point. This apparent contradiction is explained by the fact that there is no chemical interaction in a solid solution. The eutectic diagram shape depends on the difference of the A and B components' melting temperatures. If this difference is small, the eutectic point lies approximately in the middle of the diagram. If the difference is large enough the eutectic point is displaced to a composition with lower melting temperature.

This situation is however rather rare in a binary system A–B. The appropriate phase diagram, for example for the compound A_2B, is shown in Fig. 5.3. The so-called distectic point D, which corresponds to the compound, appears in the phase diagram and divides it into two eutectic phase diagrams between A–A_2B and A_2B–B, respectively.

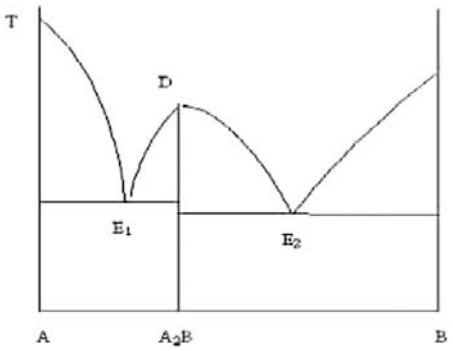

Fig. 5.3. The distectic phase diagram of a binary system with creation of the compound A_2B

5.1.3 Eutectic Phase Diagram with Areas of Solid Solutions

Quite often a stable compound does not form in a two-component system A–B. However, there is generally a high reciprocal solubility of the components in the liquid and to a lesser extent in the solid. In this case the eutectic

diagram with areas of solid solutions α and β (Fig. 5.4) can be drawn. The α and β domains correspond to the solid solution enriched with the A and B components. The areas between L, S, α, and β are L+α and L+β. When cooling the melt with a composition X, down to the temperature of the liquidus, the liquid is enriched with the B component. And then, when the liquid is displaced to the eutectic point, the crystallization of a mechanical mixture of α and β begins. The composition of each solid solution α and β corresponds to the intersection of α and S and β and S curves, respectively.

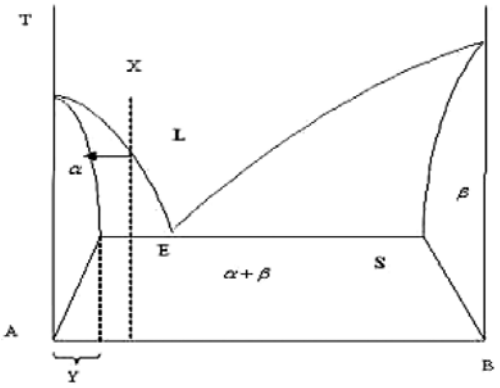

Fig. 5.4. The eutectic phase diagram of a binary system with solid solutions

5.1.4 Impurity Solubility During the Growth

There is a redistribution of impurities between the crystal and the melt during crystallization as shown in the diagrams of Fig. 5.5. Thermodynamically the impurity either decreases melting point (a), or increases it (b).

If the segregation coefficient of the impurity is smaller than 1, the melting temperature of the basic component A decreases. As seen in diagram (a) the crystallization at the temperature corresponding to the point L1 on the liquidus line results in the crystallization of a phase with a smaller impurity content than the melt. A further reduction of the crystallization temperature results in an enrichment of the impurity in both the crystal and the melt. On the other hand, for $k > 1$ the crystal is initially more rich in impurity than the melt, but the impurity concentration in both decreases when lowering the temperature (k is the segregation coefficient, i.e. the ratio of the dopant concentration in the solid state to the dopant concentration in the melt).

5.1.5 Scintillation Crystal Phase Diagrams

Several typical examples of scintillation crystal phase diagrams are discussed below. The synthesis conditions of the widely used alkali-halide scintillators,

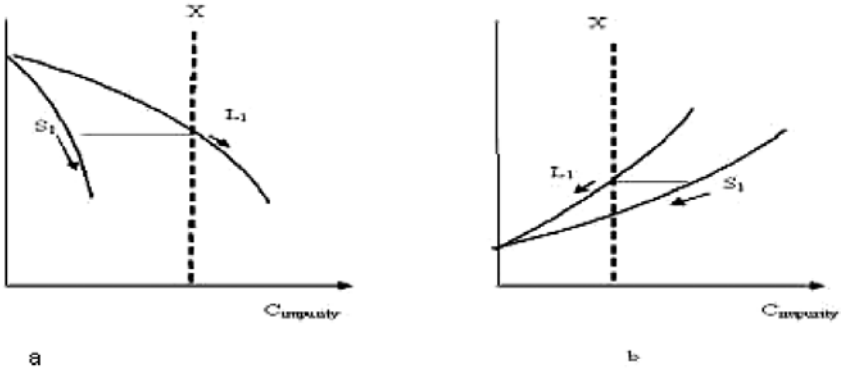

Fig. 5.5. "Crystal–melt" equilibrium in the presence of impurities

NaI and CsI, were studied in the middle of the 1970s [2]. It was shown that these crystals when doped with sodium and thallium ions form an eutectic diagram. The phase diagram of the CsI–NaI system (Fig. 5.6) results from differential thermal analysis data [3, 4] as well as from mathematical simulations [1]. Na ions solubility in the CsI lattice is limited. This limit defines the optimal level of Na doping (about 0.02%).

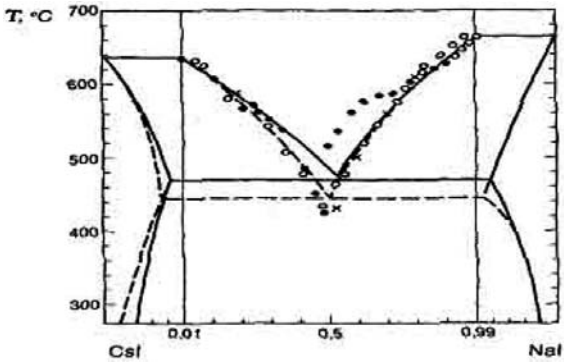

Fig. 5.6. The eutectic phase diagram for the CsI–NaI system [2–4]

The phase diagram of the PbO–WO_3 system was investigated in detail [5] and in particular on the side of a small WO_3 concentration. The study of the area enriched in tungstate anhydride is rather complicated because of the high WO_3 melting temperature and the interaction of WO_3 with the crucible material at temperatures higher than 1,100°C. Nevertheless, it is established that there is an eutectic E_1 (Fig. 5.7) between $PbWO_4$ and WO_3 with 66.5% WO_3, fusing at 930°C. There are two stable phases $PbWO_4$ and Pb_2WO_5 in this system. The other two eutectics E_2 and E_3 have melting temperatures

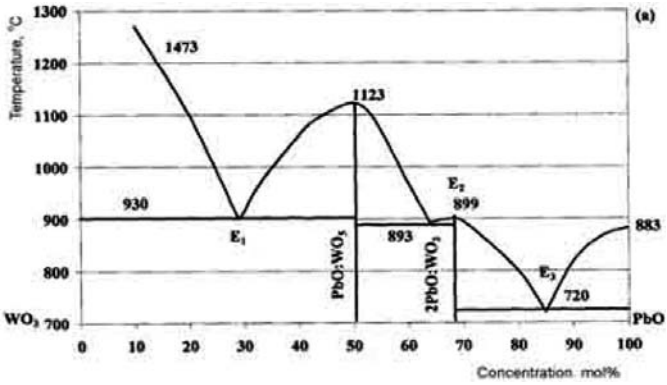

Fig. 5.7. The phase diagram of the PbO–WO_3 system

893°C and 720°C, respectively. The $PbWO_4$ melts congruently, i.e. without decomposition of the compound, at 1,123°C. The analysis of this phase diagram helps us define some practical parameters for the $PbWO_4$ crystals grown by the Czochralski method. First of all, the melting temperature restricts the choice of the crucibles to metals with higher melting points such as platinum, iridium, and their various alloys. It is also important that such crucibles do not interact with melts of similar oxides such as $PbMoO_4$, $CaMoO_4$, and $ZnWO_4$, which are impurities likely to be present in the raw material. Secondly, the possibility of using not only the stoichiometric composition of the raw material but also some excess of either WO_3 or PbO is of great importance, if it is necessary for a better tuning of the scintillation properties of the crystal. This is especially important when the properties of the grown crystals depend critically on the melt stoichiometry or when a strong differential evaporation of the different components of the melt occurs during the growth process. An initial deviation from the perfect stoichiometry can therefore be applied for the compensation of nonstoichiometry defects. The phase diagram does not provide any restriction to the relationship between the weight of the grown crystal and the weight of the initial melt in the crucible. The size of the pulled crystal is only determined by some technological constraints of the equipment such as the size of the crucible and the optimal growth technology. Some restrictions can appear because of the segregation process of additional doping ions which have segregation coefficients >1, La for instance. This doping will be pumped from the melt to the initial part of the crystal if the diameter of the pulled crystal is close to the diameter of the crucible. There is no necessity to create fast heat flow through the growing crystal or supercooling at the crystallization interface which essentially reduces the stability of the process and increases inner stresses in the crystal. A large industrial production of $PbWO_4$ by the Czochralski method [6] has been set up for the needs of the CMS experiment at CERN (see Chap. 7).

Another example of a complex phase diagram is the lutetium aluminate perovskite crystal. There are two stable phases $Lu_3Al_5O_{12}$ and $Lu_4Al_2O_9$ and a metastable phase of $LuAlO_3$ in the system. $Lu_4Al_2O_9$ is formed from oxides at temperature higher than 1,650°C and melts incongruently at 2,000°C; the most stable phase $Lu_3Al_5O_{12}$ is formed below 1,500°C and melts congruently at 2,060°C. In the $LuAlO_3$ phase diagram there is also a metastable phase in a narrow temperature range of 40°C with an incongruent melt. The low system stability is explained by the aspiration of lutetium (the lanthanide with the smallest ionic radius) into the garnet structure. From the phase diagram study one can infer that very small variations of the melt composition or temperature at the crystallization point can introduce a transition from the perovskite to the garnet phase. Therefore the size of the perovskite crystal will be severely limited if the composition of the melt and the temperature gradient are not perfectly under control at the crystallization point.

Another approach to grow this crystal is to set up the growth conditions at a high temperature gradient and a fast cooling of the crystal. The gradient provides the supercooling of the melt and maintains the composition in a metastable molten situation. This method prevents the decomposition of the solidified phase. It is experimentally confirmed that the perovskite phase $LuAlO_3$ can be obtained only by quick crystallization of the stoichiometric melt. It allows us to assume that there is a metastable variant of the phase diagram of the system in which this phase melts congruently at 1,910°C as shown in the inset of Fig. 5.8. The practical implementation of this approach to the growth of a LuAP crystal is a rather complex but manageable process.

Growing LuAP on a seeding crystal (having the same composition as the ingot) is practically impossible, as it decomposes at the contact with the melt and even a strong cooling of the seed does not give a positive result. Growing on an iridium wire is a possibility but the spontaneous crystallization is a very complex technological problem difficult to control for a consistent production. A high temperature gradient also generates important maintenance problems. The garnet phase formation at the seeding stage and during crystal growth is therefore a difficult problem for the optimization of the crystallization process. It should be noted that the first $LuAlO_3$ samples had a lot of garnet inclusions which strongly affected the scintillation performance [7].

One way to increase the domain of stability of the phase diagram is to introduce some quantity of yttrium in the lattice. The modified crystal of $Lu_{1-x}Y_xAlO_3$:Ce in which the Lu ions are replaced with Y ions have practically the same or even better scintillation performance [8, 9] as $LuAlO_3$ but with a smaller density below $8.34\,g\,cm^{-3}$ and therefore a lower photofraction. On the other hand, this composition is much more stable than the pure lutetium perovskite and its melting temperature is slightly lower. Moreover for the crystal growth of such composition it is possible to use a more stable seeding procedure with $YAlO_3$ crystals [10].

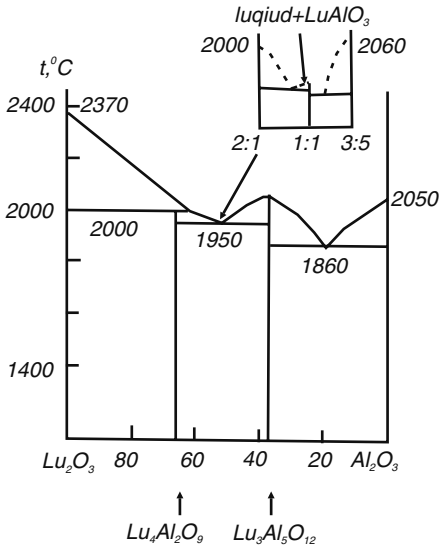

Fig. 5.8. The phase diagram of the Lu_2O_3–Al_2O_3 system. The inset shows the details in the region of the 1:1 ($LuAlO_3$) compound

5.2 Single Crystal Growth

Although most of the applications require their use in a single-crystalline form, inorganic scintillators are used in a large variety of types and shapes. This fact requires a special attention to methods, technologies, and equipment for the single crystal growth. It is worth mentioning that the physics and technology of crystal growth do not depend on their subsequent application. But the specific character of the applications imposes quite often some requirements on the growth process, namely, for dimensions and homogeneity of optical properties, purity of the initial material and activator uniformity distribution, composition stoichiometric, and minimum concentration of point and linear defects.

5.2.1 General Considerations on the Crystallization Process

In general, crystallization is viewed as the formation of a new solid phase in melts, solutions, solid substances, and gases. The formation of a new solid phase can occur both inside the initial phase and on the phase surface. The causes of the new phase formation are critical supersaturating, critical overcooling, or nucleation. A stable nucleus is characterized by a critical size and it takes a definite form defined by the minimum surface energy that can be reached for a given volume. From the theory [11] one can calculate the critical nucleus size and its formation energy, define the relation between the critical supersaturation and the heat of the melt, and consider the effects of diffusion

and heat transfer processes, i.e. describe the kinetics of phases interaction. This allows us to optimize the crystallization process and to grow good quality crystals even at rather high rate of mass production. For the growth of single crystals there must be a unique nucleus; otherwise a multiple nucleation will produce a polycrystal. Various techniques and methods are used to allow the growth of one nucleus only or to select a single nucleus from several ones during the crystallization process. The simplest method is the crystal growth from a previously prepared seed. The seed crystal is usually cut from the same crystal, but it is sometimes possible to use a single crystal of different composition.

Several papers and books describe the basic theoretical principles of single crystal nucleation, growth and growth principles and procedures [2, 11–13]. That is why we shall consider here only a few important aspects of the scintillation single crystal growth.

5.2.2 Basic Methods for Scintillation Crystal Growth

The core of almost all crystal growth methods is the principle of oriented crystallization. Its basic feature is the balance of two different processes: heat transfer and crystal interface transfer.

The methods of crystal growth are usually classified according to the following conditions:

- phase status and composition of the initial phase;
- type of the process driving force (temperature gradient or concentration, or pressure).
- Starting from the first point it is possible to grow single crystals:
- from melts;
- from solutions;
- from gas phase;
- by phase transformations in solid phase.

The classification of the methods within these groups is carried out according to the second point. The temperature gradient is mainly used as the driving force of crystallization. Several methods are used which differ in the way the heat transfer and the hydrodynamic conditions are applied. They are

- creation of temperature gradient between the crystal and the melt by heat transfer from the seed;
- creation of temperature gradient between the crystal and the melt by heat transfer from the seed and pulling up the grown crystal from the melt (Czochralski and Kyropoulos's methods);
- floating temperature gradient through the melt (Bridgeman and Stockbarger's methods), etc.

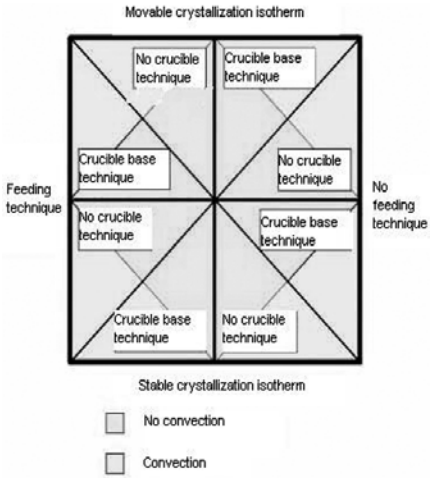

Fig. 5.9. A classification of crystal growth methods

The methods of crystallization are often classified according to such criterion as the presence or absence of a melting pot (crucible). Figure 5.9 illustrates a typical combined classification. Various technical solutions are available to grow single crystals. The implementation of a growing method is characterized by technological features, equipment design, and phase diagram peculiarities.

Finally, one more pragmatic selection criterion of the single crystal growth method concerns the single crystal nucleation and the shaping of the ingot. Through the combination of all these criteria all the methods can be divided into two groups:

- single crystal growth in ampoules such as Bridgeman, Stockbarger, Stoeber [14, 15] and
- single crystal pulling from melt such as Kyropolos, Czochralski, etc. [16, 17].

Below we describe the basic principles of these methods.

5.2.3 Bridgeman and Stockbarger Methods

The external form of the crystals grown in ampoules is strictly set by the geometry of the ampoule (as a rule, it is cylindrical, although, sometimes rectangular ampoules are also used). The growth of complex shape crystals is limited by the necessity of crystal extraction from the ampoule which can be complicated by the adhesion of the crystal material to the ampoule material. (It should be noted that, for this reason, the crystals are subject to deformation during the cooling which induces intrinsic stress in them.)

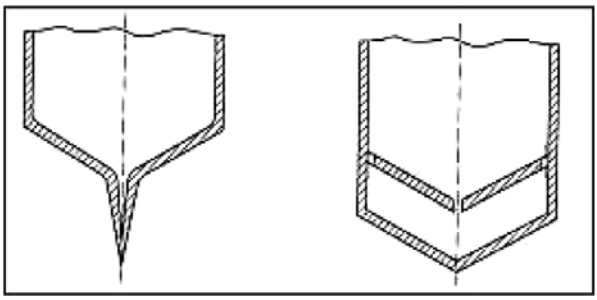

Fig. 5.10. Ampoulous shape for single nucleus selection and single crystal growth [2]

One of the most complex problems of this group of methods is the spontaneous crystallization on the ampoule surface. As a result, the orientation of the crystal is difficult to control. For example, scintillation single crystals of NaI(Tl) have the spontaneous orientation (110) [2], when grown by the Stockbarger method in quartz ampoules, regardless of the speed of growth and of the ampoules shape. Figure 5.10 illustrates the typical shapes of ampoules for the oriented single crystals growth. The single crystal growth is achieved by setting the conditions for the preferred growth orientation or by the use of a well-oriented seed.

A good control of the heat transfer process is a fundamental aspect of single crystal growth technology. The temperature gradient or the homogeneity of the thermal field (radial or axial in relation to the growth of a single crystal) is the driving force of the crystal growth process. Consequently, all the crystal growing furnace elements (heaters, screens, gaseous medium, etc.) act as the main control elements of the crystallization process. Figure 5.11 b shows

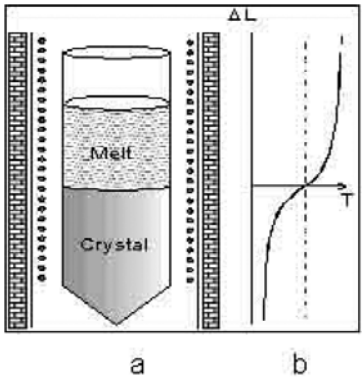

Fig. 5.11. Stockbarger method scheme (**a**) and temperature distribution along the furnace (**b**)

the diagram of the temperature field axial distribution for the Stockbarger method. Figure 5.11a illustrates the corresponding layout for this growing method.

Initially, the raw material is placed in the higher temperatures area (where it melts). The crucible (ampoule) is moved through the thermal gradient zone, where the temperature is lowered below the melting point. This is the area where the crystallization takes place. The volume of the melt will therefore decrease continuously and the growing crystal starts substituting for the melt. It follows that the temperature field parameters change during the crystal growth. The amplitude of these changes is determined by both the configuration of the initial thermal field and the changes in the crystallization process. The system has a nonconservative character because there are losses at the melt–gaseous medium interface besides mass transfer at the melt–crystal interface. As a general rule, when developing a single crystal growth technology it is good to bear in mind that the system is open and is nonconservative in the sense that the losses of separate components are irreversible. The basic principles of crystallization processes in totally open systems are explained in [2]. As the thermal field in the growing crystal system is continuously changing the main problem for all the crystal growth technologies is to find a method to adapt the conditions of heat and mass transfer, which is usually done empirically by a trial and error approach.

A long practice and experience has been accumulated over the years and halide scintillators, for example, NaI (Tl), CsI (Tl), CsI (Na), are successfully grown by the Stockbarger method. This method is also widely used for growing oxide scintillation crystals [18]. The simplicity and relatively low production cost of this method make it very practical for search and synthesis of new scintillation crystals. The principle and basic components of the crystal growing furnace remained almost unchanged since the invention of this method. It comprises two chambers with self-contained top and bottom heaters. The sharp thermal gradient is produced by a diaphragm. The influence of the water-chilled support of the ampoule on the temperature gradient is negligible. The temperature gradient in the furnace exceeds $10^{\circ}\mathrm{C\ cm^{-1}}$. As a rule, the rate of the ampoule transfer does not exceed 1 mm $\mathrm{h^{-1}}$.

If the simplicity and reliability of the Bridgeman and Stockbarger designs make them particularly attractive for many applications these methods are however rather inconvenient for a good homogeneity especially for doped single crystals. A high gradient of the doping impurities is observed in these crystals. The consequence is to reduce the production yield as only a fraction of the ingot can be generally used.

5.2.4 Czochralski and Kyropolos Growth Techniques

When pulling a seeded single crystal from the melt the crucible shape and size do not have a direct influence on those of the crystal. The crystal shape instead is determined only by the parameters of the growth process (mass and

heat transfer, above all). A seed crystal is a prerequisite of these methods. Its crystallographic orientation is transferred to the crystal and is a determining factor for the whole ingot size and quality.

There are two fundamental methods to grow crystals from the melt.

In the classical Kyropolos method [16] the entire crystallization process starts with the seeding and propagates through the melt as a result of a continuous temperature decrease applied during the process. There is no relative movement of the seed and the crucible.

In the Czochralski method [17] the crystal is pulled from the melt. This method is the most widely used for growing oxide scintillators (since virtually all known oxides are produced by this method) as well as for many other scintillators.

The Czochralski growth method is an example of heterogeneous crystallization which takes place at the crystal–melt interface. The crystallization practically starts from the seed crystal. Contrary to the Kiropoulos method the crystal is continuously pulled from the melt and rotates during the growth which helps maintain a good mixing of the melt (Fig. 5.12). The driving force of the process is the temperature gradient at the phase boundary. The temperature gradient determines all the main characteristics of the growth process: crystallization rate, crystal size, and crystallization interface shape. For a constant temperature gradient the pulling rate and crystallization rate should coincide. If the pulling rate is less than the growth rate the crystal increases in diameter and vice versa. This provides the technological means to control the shape of the crystal.

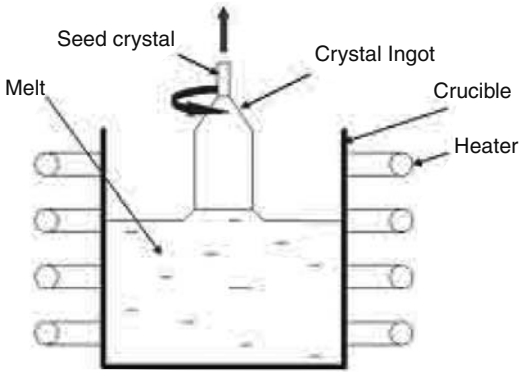

Fig. 5.12. The Czochralski growth method

Crystal pulling and gradient control should be carried out rather smoothly in order to maintain the stability of the process. A sharp increase of the pulling rate can result in the separation of the crystal from the melt and in the discontinuation of the crystallization process. In contrast, a sharp decrease

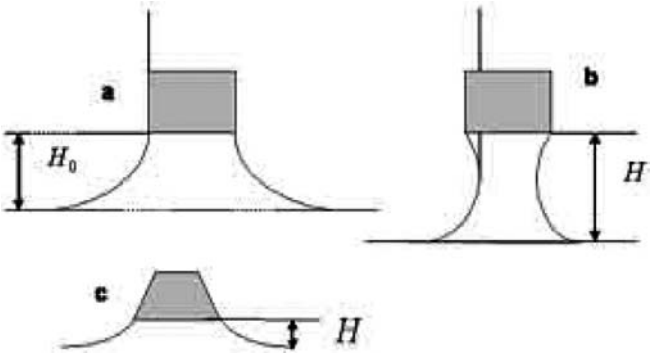

Fig. 5.13. The form of the melt meniscus in the Czochralski method

of the pulling rate will result in the increase of the crystal diameter with an increased risk of polycrystal growth. To provide a stable crystal growth process it is necessary to fix the crystallization interface and the shape of the meniscus of the melt (Fig. 5.13). The meniscus shape is defined by the balance between the surface tension and the weight of the column of the melt lifted to the altitude H:

$$\sigma \left(\frac{1}{R_1} + \frac{1}{R_2} \right) = \rho_{\mathrm{l}} g H \ , \tag{5.1}$$

where σ is the surface tension coefficient; R_1 is the radius of the meniscus curvature in one direction, R_2 is the radius of the meniscus curvature in the perpendicular direction; ρ_{l} is the melt density, and g is the gravity coefficient.

For crystals of diameters much bigger than the height of the meniscus the altitude of the column H_0 at which the growth with a constant diameter can occur is given by

$$H_0 = \sqrt{\frac{2}{\rho_{\mathrm{l}} g}} \ . \tag{5.2}$$

If the crystallization interface is higher than the point H_0 the crystal diameter will be smaller (Fig. 5.13b) and vice versa if it is lower than H_0 (Fig. 5.13c). In practice, however, the operator does not adjust the critical position of the crystallization interface as a function of the meniscus shape. It is in fact easier to adjust and control the temperature and the temperature gradients of the system. It is easy to understand this approach by the analysis of the thermal balance equation at the crystallization interface. First of all there is a heat transfer between the hot liquid and the crystal which is cooler but also the emission of the latent crystallization heat through the crystallization interface. In the first approximation (regardless of the crystal thermal conductivity anisotropy, thermal field asymmetry, and so on) the equation of thermal balance is given by

$$\rho_{\mathrm{s}} V Q = \lambda_{\mathrm{s}} \left(\frac{\mathrm{d}T}{\mathrm{d}X} \right)_{\mathrm{s}} - \lambda_{\mathrm{l}} \left(\frac{\mathrm{d}T}{\mathrm{d}X} \right)_{\mathrm{l}} , \tag{5.3}$$

where ρ_{s} is the density of a crystal, V is the crystallization rate, Q is the latent crystallization heat, λ_{s} and λ_{l} are the thermal conductivities of solid and liquid phases, respectively, and $(\mathrm{d}T/\mathrm{d}X)_{\mathrm{s}}$ and $(\mathrm{d}T/\mathrm{d}X)_{\mathrm{l}}$ are the temperature gradients in solid and liquid phases at the phase boundary, respectively.

From the equation it appears that the maximum crystallization rate is obtained for a minimal gradient in the melt (for example, due to good mixing) and a maximum gradient in the crystal. It is obvious that substances of high thermal conductivity can grow faster than substances of low thermal conductivity. So metals are grown at higher speeds than ionic (dielectric) crystals. More detailed studies of the thermal balance at the phase boundary requires the consideration of many parameters [2, 19, 20]. This may include the heat transfer due to IR emission. It is particularly important for crystals of high melting point because radiative loss is proportional to the fourth degree of the temperature. The form of crystallization interface (flat, convex in melt or concave in the crystal) also influences the result of the analytical solution of the thermal balance equation [2].

5.2.5 Modern Trends in Scintillation Crystal Manufacturing

The last decade has seen new developments of great interest in the understanding of scintillation physics and in the engineering of scintillators. This has been triggered in particular by the increasing demand for HEP and nuclear medicine. The scale of scintillation single crystal production is nearly two orders of magnitude smaller than the scale of semiconductors (such as silicon) manufacturing, but the requirements for crystal dimensions for gamma-ray detection is extremely high [21]. For instance, a full-size crystal for SPECT system reaches $600 \times 500\,\mathrm{mm}^2$ (see Fig. 5.14). Not even mentioning the issue of homogeneity of the scintillation parameters on such a large surface, it is clear that crystals of this size cannot be produced by the above-mentioned methods. All of them are limited regarding the crystal dimensions both geometrically (for example, ampoules in the Stockbarger and Bridgeman methods) and technologically (due to the difficulties in creating the thermal field to ensure a sustainable crystal growth).

5.2.5.1 Large-Size Alkali-Halide Scintillation Crystal Growth

Since the middle of the 1980s a large R&D effort has been spent for large-size crystal pulling methods. The progress in this field has open new possibilities for nuclear medicine cameras.

A major attention has been paid to methods of continuous growth to produce large-size scintillation crystals. It should be mentioned that at the same time a number of projects have emerged for developing continuous pulling

Fig. 5.14. Scintillator for the conventional SPECT system

methods for semiconductors (silicon; for instance see [22, 23]). The case of scintillators, however, has proven to be more complicated. The main reason is the need to provide a regular distribution of the activator impurity along the whole crystal length.

In the practice of homogenous scintillation growth this effort has led to the implementation of the modified Czochralski–Kyropoulos techniques. The essence of the concept is based on a continuous feeding of the melt to compensate its reduction during the single crystal pulling process. The balance between the crystal and the melt is maintained by feeding new raw material in powder or already prepared in the liquid phase.

Figure 5.15 shows the scheme of an installation for continuous large-size alkali-halide single crystal growth with powder feeding [24]. The crucible has a special shape for allowing a continuous and gradual powder feeding. Once molten the additional raw material is transferred to a quite large crucible and rapidly homogenizes due to melt convection.

This technique is not too difficult to operate. In the simplest case the task is simply to maintain a steady crystallization rate (that is to maintain a uniform cross-section and axial growth rate).

$$\begin{aligned} \frac{\mathrm{d}\nu_{\mathrm{S}}}{\mathrm{d}t} &= 0 \,, \\ \frac{\mathrm{d}S_{\mathrm{S}}}{\mathrm{d}t} &= 0 \,, \end{aligned} \tag{5.4}$$

where V_{S} is the axial growth rate and S_{S} is the crystal cross-section.

In the case for which mass transfer is conducted through the crystal melt interface, it means that

$$\frac{\mathrm{d}m_{\mathrm{l}}}{\mathrm{d}t} = \frac{\mathrm{d}m_{\mathrm{s}}}{\mathrm{d}t} \,, \tag{5.5}$$

where $m_{\mathrm{S}}, m_{\mathrm{l}}$ are the masses of the crystal and melt, respectively.

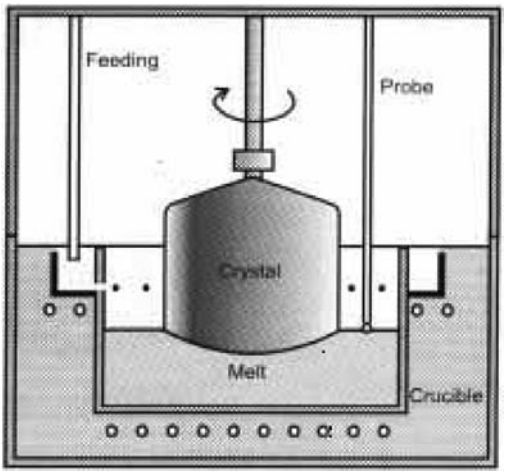

Fig. 5.15. Scheme of a continuous growth technique with the powder feeding system

From (5.4)–(5.5),

$$\frac{\mathrm{d}^2 m_\mathrm{s}}{\mathrm{d}t^2} = \rho_\mathrm{s}\left(\mathrm{s}\frac{\mathrm{d}V}{\mathrm{d}t} + V\frac{\mathrm{d}s}{\mathrm{d}t}\right) = \frac{\mathrm{d}^2 m_\mathrm{l}}{\mathrm{d}t^2}\ , \tag{5.6}$$

where ρ_s is the crystal density.

To pull a crystal at V_s, S_s = const it is necessary to monitor several parameters with the following equipment:

(i) V_s = const: crystal length gauge, melt level control,
(ii) S_s = const: crystal diameter control,
(iii) $\frac{\mathrm{d}m_\mathrm{l}}{\mathrm{d}t}$ = const: the melt weight control, the melt level control,
(iv) $\frac{\mathrm{d}m_\mathrm{s}}{\mathrm{d}t}$ = const: crystal weight control.

Figure 5.16 shows the regulation of the continuous crystal pulling process based on melt level monitoring. For this purpose the oven is equipped with an electric contact sensor responding to the interruption of a circuit when the melt level decreases in the crucible. The accuracy of such a sensor is limited by the meniscus height generated at the sensor's edge. The sensor signal is coupled to the feeding block, which restores the melt level by adding new raw material into the crucible.

One of the most important aspects of the raw material feeding method is to provide a continuous control of the growth process. Any crystallization speed jump (regardless of the initial causes, including temperature jump, melt level jump, etc.) leads to an instantaneous crystallization speed change. Depending on the amplitude of the perturbation this will lead to the creation of intrinsic crystal structure defects as well as activator distribution

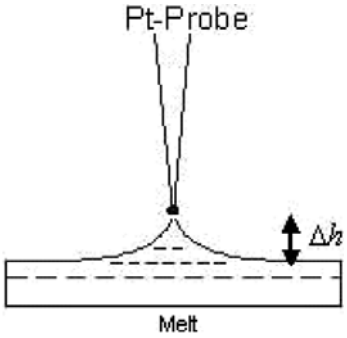

Fig. 5.16. Melt level control scheme with electric contact Pt probe

nonuniformity in the crystal, inclusion of impurities, and capture of the gases dissolved in the melt. It is therefore essential to keep the feeding process as continuous as possible. This procedure is described in detail in [13].

As a first approximation (steady-state process) the crystal diameter is given by the expression

$$d = 2\left(\frac{m}{\pi\rho_{\mathrm{s}}V_{\mathrm{p}}}\right)^{\frac{1}{2}} \tag{5.7}$$

where ρ_{s} is the crystal density, m is the feeding rate, and V_{p} is the pulling rate.

As a second approximation [2], additional factors should be taken into account, for example, single crystal creation and evolution under the melt surface, and material loss due to evaporation from the free surface area of the melt. In general, every such detail makes the control algorithm more complex, but does not affect the system control stability.

The method of automated crystal growth with a melt feeding system is also well known [2, 13, 24, 25]. This method is based on crystal and raw material weight balance equations, but possesses a number of specific features. The essence of this method is the process of pulling the crystal from a small conical crucible (which reduces the evaporation of the initial substance and the activator). Molten raw material is continuously fed from a special toroidal crucible. Figure 5.17 illustrates the main features of this technique.

The concept of the method is presented in Fig. 5.18. The initial stage of radial growth starts in the lowest part of a conical crucible where the melt surface diameter is comparable to the seed crystal diameter. At the radial growth stage a crystal is being pulled at the speed V_{p}. Simultaneously, the melt level is elevated at a rate V_{l} by feeding the raw material at the $\mathrm{d}m/\mathrm{d}t$ mass rate, so that $V_{\mathrm{p}} > V_{\mathrm{l}}$. This is the phase of the continuous diameter increase of the ingot to produce a nice conical shape from the seed to the required diameter ingot (stages b–d, in Fig. 5.18). The melt temperature is adjusted so that the linear speed of the radial growth is essentially equal to that of the melt surface diameter increase. Thus the radial growth from the

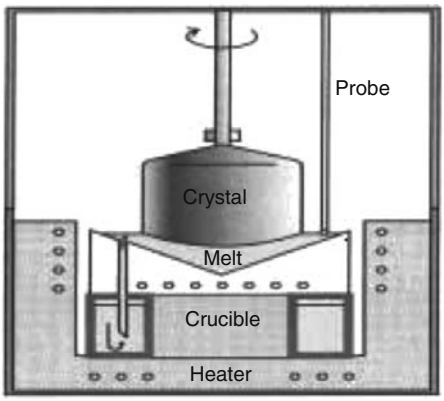

Fig. 5.17. Continuous growth technique with the melt feeding system and RAP (reactive atmosphere processing) capability [25]

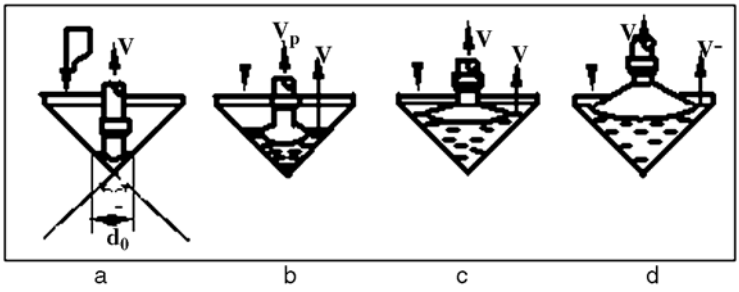

Fig. 5.18. Crystal growth from the conical crucible with the melt level control

seed diameter to the final value of the single crystal ingot is performed by minimizing the free melt surface. It is very important to prevent evaporation of the activator (Tl ions for NaI or CsI crystals) and to maintain a permanent Tl concentration in the melt.

These techniques allow us to combine a lot of specific features which are important for the optimization of scintillation single crystal growth:

1. continuous growth of large-size single crystals;
2. fixed "crystal–melt" interface, i.e. constant growth conditions on the solidifying interface;
3. possibility of raw material and activator feeding;
4. bulky crucibles that allow us to provide a good melt convection (and homogenization);
5. simple control method based on electro-contact probe;
6. possibility of rotating both the crystal and the crucible loaded with melt, allowing a good melt homogenization and maintaining a perfect symmetry of the thermal fields in the growing crystal;

7. extra raw material purification (such as RAP (reactive atmosphere processing) atmosphere treatment);
8. melt feeding, i.e. doping with activated melt.

A number of algorithms of large-size crystal production and technically modified systems for this production are presented in [2]. A typical single crystal ingot is shown in Fig. 5.19. Equipment and alkali-halide single crystal growth techniques are described in detail in [2]. At present these methods are commercially applied for producing NaI(Tl), CsI(Na), CsI(Tl), CsI(pure) single crystal up to 600 mm in diameter and up to 750 mm in height. The total weight of such ingots reaches 400–500 kg.

Fig. 5.19. Large-size halide scintillation single crystal ingot (Courtesy of Amcrys-H, Ltd)

5.2.5.2 Oxide Scintillator Single Crystal Growth

Oxide crystals have in general a tendency toward faceting the interface surface due to the different growth kinetics in various crystallography orientations [26]. As a result the interface can be either round or faceted depending on the growth conditions. Two opposite approaches are used to grow crystals such as $Bi_4Ge_3O_{12}$ (BGO), $CdWO_4$ (CWO), and so on. The conventional Czochralski method (CZ) [29] is based on high temperature gradients to suppress the facets formation. The final ingot is round in shape. An alternative way is the low temperature gradient CZ growth technology [27]. In this case the interface shape is fully faceted [28]. The essential features of this technique are shown in

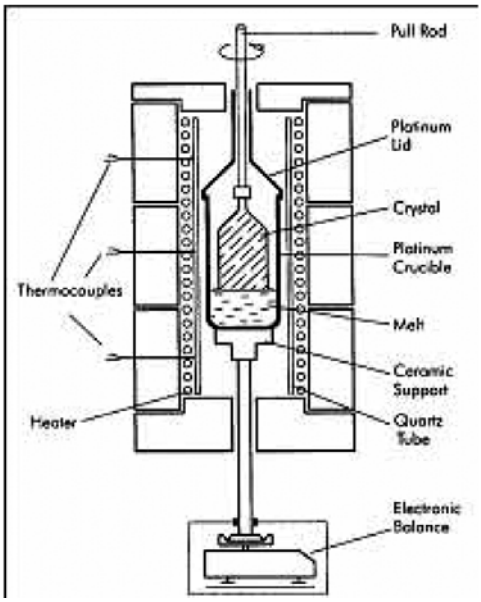

Fig. 5.20. Low gradient Czochralski technique [27]

Fig. 5.20. A special platinum crucible inside the multizone heater allows us to sustain and control axial and radial gradients to about 0.05–1.0°C cm^{-1}. The technique includes the weight control system and is fully automated growth procedure as the visual control is impossible [27]. The quality of the crystal depends on the orientation of the growth direction ({211} plates family or [100]/[111] directions for BGO, for example [27, 28]). As a result, large-size oxide scintillators of diameter up to 180 mm and length up to 350 mm have been grown with this technique.

The reliability and stability of the crystal growth process are essential to maintain a good homogeneity of the scintillator parameters. This aspect has been the focus of all the development efforts on the growth technology of $PbWO_4$ (PWO) for the Large Hadron Collider (LHC) at CERN. In this particular case the technology of conventional large gradient CZ growth has been chosen. Since this is one of the most vivid examples of a large world-wide technological effort on a scintillator we will use PWO to illustrate some aspects of the choice and tuning of the technology to satisfy the end user's requirements. The main challenge in this case was not so much to grow crystals of the right dimensions, but to guarantee a good radial and longitudinal homogeneity within the boules and to ensure a high reproducibility from ingot to ingot.

The result of this unprecedented R&D effort in the field of scintillators is that several tens of thousands single PWO crystals have been grown with a length of 290–310 mm (including the growing cone) and a cross-section of

36–40 mm. Moreover excellent quality ingots up to a diameter of 100 mm can be grown. It is supposed that crystals are annealed in air during industrial production. The detailed description of the crystal growth process is given in [6].

The most important requirements for the PWO crystal growth are as follows:

- The use of a stoichiometric mixture of tungsten oxide WO_3 and Pb_3O_4. The main reason for this choice is to create an excess of oxygen in the melt while growing the crystals in an atmosphere depleted in oxygen.
- Growing in gas atmosphere depleted in oxygen in order to prevent the oxidization of some of the lead ions in the trivalent state. It is now well established that PWO single crystals grown in air in composition contain trivalent lead ions which cause yellow coloration of the crystal.
- Orientation of the seed along the crystallographic axis "a." This allows us to reduce the radial stress in the ingot which results in a better mechanical stability and considerably simplifies the process of mechanical machining.

To increase the efficiency of raw material conversion into the crystalline mass, it is necessary to proceed to several sequential crystallizations from one crucible by means of raw material refilling after each growth process. The possibility of reprocessing rejected crystals as well as waste from mechanical processing is also an important aspect of the economy of the production. Such an approach allows us to bring the coefficient of raw material effective use up to 85%. However, the increasing number of crystallizations in crystals results in a progressive increase of defect concentration. It has been demonstrated that up to 15 successive crystallizations can be made with crystals of 40 mm diameter with a good reproducibility of their parameters if a proper tuning of the stoichiometric composition is made at each refill.

Raw Material Purity

The purity and preparation of the raw material plays a considerable role too, particularly if one wants to have radiation hard crystals. The amount of some impurities such as Li, Be, B, F, Mg, Cl, Mn, Ni, Co, As, Zr, Sr, Rb, Ge, Ga must not exceed 0.05 ppm, the amount of Na, Al, S, Zn should be less than 0.5 ppm, and the amount of P, Ti, V, Cr, Cu should be less than 0.1 ppm.

Crucible Filling

The filling of a crucible with raw materials presents a number of difficulties. The density of the powder being much smaller than the density of the melt, one has to proceed in several steps which results in lengthening the crystal growth cycle and in increasing the danger of raw material contamination with impurities. There are several methods of raw material densification. The easiest and the most commonly used one is tabletting. The raw material is mixed with filling agents (for example, alcohol) and pressed in the form of

tablets matching the size of the crucible. The tablets are then calcinated at a temperature ensuring a maximal mechanical strength and elimination of residues or even traces of the binder. In many cases the density of the tablets may reach up to 70% of the crystal density.

Another approach is the granulation technique. The liquified raw material is exposed to a cold air stream. This method makes it possible to bring the raw material density up to 85–90% of the crystal density.

There is also a possibility of filling the crucible by means of special loading devices. This technique may be realized on separate installations or use specific devices built into the growth installations. An example of such an approach is illustrated in Fig. 5.21. The raw material is spilled into the platinum crucible, and then heated until melting, after which the melt is poured out into a platinum mold. In the process of melt crystallization one can obtain tablets with a density up to 8, close to the PWO single crystal density (8.28), and a diameter 5–6 mm smaller than the inner diameter of the growth crucible.

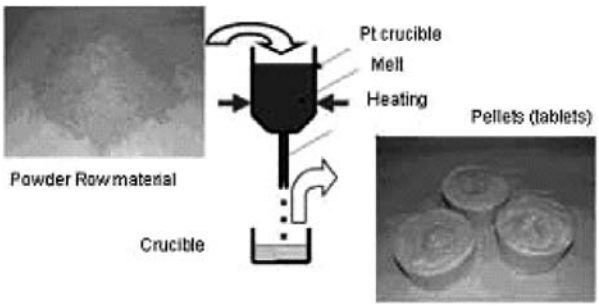

Fig. 5.21. Raw material preparation scheme

The Choice of the Crucible Material

It is an extremely important task to select the optimal crucible for crystal growth because the use of semiprecious metals such as platinum or iridium has a strong impact on the crystal price. The crucible cost reaches 20–50% of the crystal cost and can be even higher for crystals with a higher melting temperature.

The main requirements for the choice of the crucible material are

- metal resistance to the interaction with melt;
- metal cost and availability;
- thermal stability of crucibles and resistance to deformation under thermocycling;
- immunity to atmosphere conditions;

- lifetime and reprocessing capability.

Various kinds of crucibles are used for the Czochralski single crystal growth process. As a general rule, for crystals with melting point below 1,500–1600°C platinum crucibles are used while iridium crucibles are applied for crystals of higher melting points.

In the case of the PWO industrial crystal production optimization, the tuning of the crucible design has allowed an increase of its lifetime up to 8,000 h, i.e. about 1.5 years. Besides, there is a need for an optimization of the form, dimensions, and constructions methods of the crucibles to answer the technical and economic mass production challenges. Two ways have been explored to solve these problems. The first one was to make as thin as possible the side wall of a conventional welded crucible. The second one was to develop a combined platinum–ceramic crucible. A platinum crucible (the inside of which is in contact with the melt) has no joints. It is produced from a 0.6 mm platinum sheet by deep drawing method. The outside of a combined crucible is made of a 2–3 mm aluminum-based ceramics protective coating which is applied over the platinum base by plasma spraying. This construction reduces the platinum loss during the crystal growth process.

For LuAP, LuYAP, LSO, and LYSO scintillation crystals the choice of the crucible is very critical since the melt is characterized by high values of density, melting point, activity, and fluidity. High temperature gradients result in overheating the crucible. The local overheating of the crucible may damage it and result in leaking of the melt. This is one of the main difficulties for growing LuAP and LSO as well as other crystals with a high temperature melting point.

5.2.6 State-of-the-Art for Crystal Growth

In spite of a high automation of the crystal growth process these technologies still remain sometimes more art than science. The state-of-the-art of these technologies determines both the efficiency of the production and the quality of the scintillators. Figure 5.22 shows PWO crystals of different dimensions grown by the Czochralski method with platinum crucible of 130 to 150 mm diameter.

One of the examples of this symbiosis between art and science is the growth of highly transparent single crystals which requires not only a good knowledge of fundamental principles but also a long trial and error experience. It is evident that crystal properties are to a large extent related to the level of impurities which are introduced in the crystal from the melt. These impurities can be either uncontrolled or introduced on purpose in the crystal during the process. But in both cases it is necessary to consider the heat transfer and the diffusion process together. When growing a crystal with a speed different from zero, the concentration of impurities in the melt is a

Fig. 5.22. PWO single crystal grown by the Czochralski method

dynamic process. The corresponding inhomogeneity of the impurity distribution is determined by the diffusion speed and by the limited efficiency of hydrodynamic mixing. Figure 5.23 illustrates the effect of overcooling by excess of impurity concentration. The temperature of crystallization depends on the impurity concentration. The balanced liquidus temperature (crystallization temperature) T_l and the actual temperature gradient (determined by the equipment) can be rather different. If the actual temperature gradient crosses the solidification temperatures line (gradient I in Fig. 5.23), the melt on the crystallization front appears to be overcooled. It creates the conditions for multicrystallization and polycrystal growing centers appear. This is called the effect of "concentration overcooling." The crystallization front loses its stability.

To avoid the negative influence of concentration overcooling the temperature gradient $\mathrm{d}T/\mathrm{d}X$ must lie higher than the liquidus temperature curve, i.e. $\mathrm{d}T/\mathrm{d}X \geq (\mathrm{d}T/\mathrm{d}X)_{X=0}$. This defines the following condition:

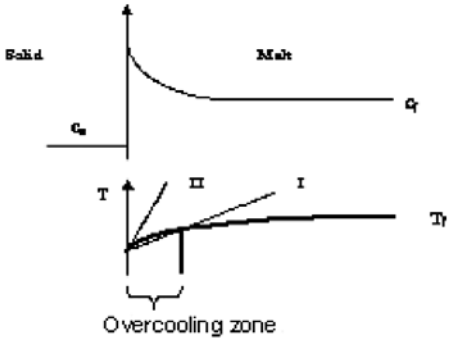

Fig. 5.23. The distribution of impurity C_l and temperature T_l at the crystallization front for the case $k_0 < 1$

$$\frac{\mathrm{d}T}{\mathrm{d}X} \geq m\frac{c_\mathrm{s}V(1-k_0)}{k_0 D}\ , \tag{5.8}$$

where k_0 is the segregation coefficient, D is the diffusion coefficient, and m is the coefficient of melting temperature decrease as a function of impurity concentration (linear approximation).

The typical signature of such instabilities (concentration overcooling) is

- a cellular growth, i.e. the phenomenon when the smooth surface of the crystallization front is broken into separate fragments and
- the probability of impurity trapping, forming a striation structure.

Figure 5.24 shows an example of such a kind of micro striation, visualized by the scattering of light by the entrapped particles.

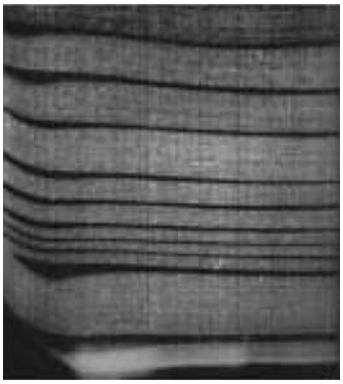

Fig. 5.24. Striation picture in grown crystals [30]

Naturally such kinds of artifacts influence the light propagation inside the crystal and at the end reduces the scintillation efficiency of the material.

There are very few descriptions of the state-of-the-art recipes for scintillation crystal growth. A few reviews related to the industrial approaches for LSO growth are for example given in [31, 32].

5.3 Activator Distribution in a Single Crystal

As was mentioned in previous chapters the scintillation mechanism in several scintillating crystals involves activator ions which are introduced as doping ions in the lattice. To manage an optimal activator concentration in the crystal the understanding of the impurity distribution process in the crystal ingot is therefore important.

Even small changes in the conditions of crystallization can induce large doping concentration variations in the crystal and result in nonuniform scintillation characteristics of the material. This problem is typical for all activated scintillators growth techniques and impose a great care on impurity selection, crystal doping conditions, and concentration control methods.

In the case of Czochralski growth, for one doping ion with a segregation coefficient $k_0 < 1$, a low evaporation rate, no pollution problems and with a diffusion rate in the liquid phase much higher than the crystallization rate, the impurity distribution is adequately represented by the Pfann (5.9) [14]. For a simple crystallization model without continuous feeding of the dopant the concentration profile is shown in Fig. 5.25.

$$C_\mathrm{s} = \frac{\kappa_0 C_0}{1-(1-\kappa_0)g} \,, \tag{5.9}$$

where g is the crystallized melt share, C_s is the impurity concentration in the melt at some point, C_0 is the initial impurity concentration in the melt, and k_0 is the segregation coefficient.

If the technical requirements impose a limit on the impurity nonuniformity along the length of a crystal,

$$\frac{c_\mathrm{bottom}}{c_\mathrm{top}} \leq \alpha \,, \tag{5.10}$$

provided that the crystallization interface is flat and that the weight of the initial cone weight is small as compared to the weight of the cylindrical part of the ingot, the optimum crystal dimensions are

$$L_\mathrm{c} d^2 = \frac{4M_0}{\pi\rho_\mathrm{s}}(1 - \sqrt[k_0-1]{\alpha}) \,, \tag{5.11}$$

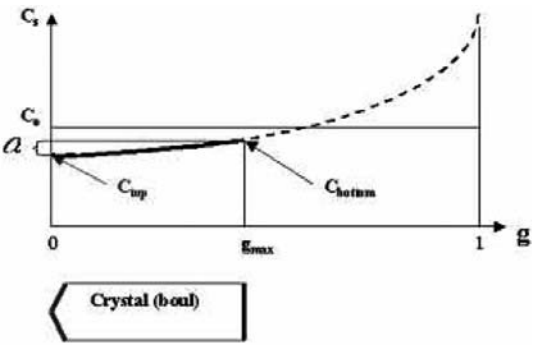

Fig. 5.25. Impurity distribution along the length of a crystal ingot

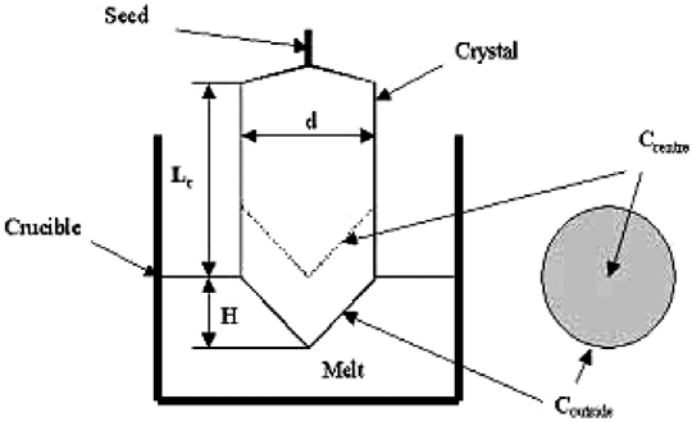

Fig. 5.26. Impurity distribution along the crystal cross-section

where L_c is the length of the crystal cylindrical part, d is the diameter of the crystal cylindrical part, M_0 is the weight of the initial melt, ρ_s is the crystal density.

However, as shown in Fig. 5.26, impurity segregation occurs not only along the length, but also along the cross-section of the crystal. If the crystallization interface is not flat the concentration profile along the crystal cross-section will depend on its curvature as well as on the crystal length and diameter.

If the technical requirements impose a limit on the impurity nonuniformity across the crystal,

$$\frac{c_{\text{outside}}}{c_{\text{center}}} \leq \beta \, . \tag{5.12}$$

In this case the ratio of the optimum crystal length, diameter and height of the crystallization interface convexity will be as follows:

$$L_c = \frac{4M_0}{\pi \rho_s d^2} - H\left(\frac{1}{1 - \sqrt[k_0 - 1]{\beta}} - \frac{2}{3}\right) \, . \tag{5.13}$$

The best solution to obtain a uniform activator distribution is therefore activator feeding during the growth process. Continuous growth allows us to control the impurity content in the melt thereby giving an opportunity to obtain scintillators with a uniform activator distribution in the whole ingot. The Tl distribution uniformity in grown CsI(Tl) crystals does not exceed $\pm$ 6% [2]. This is also a good way to compensate the evaporation from the melt in the case it is important, as it is for Tl in NaI(Tl) and CsI(Tl) crystals [2].

With this procedure of continuous growth with feeding it is possible to obtain single crystals of very large size with a good uniformity of the scintillation parameters.

5.4 Raw Material Preparation for Scintillator Crystal Growth

As was mentioned in Sect. 5.2.5 the quality and the preparation of the raw material play a very important role for the growth of oxide crystals for scintillator applications. This is even more important for alkali-halide scintillators. Many factors need to be considered to define the specifications and the conditions of scintillation single crystals growth. Using the example of the alkali-halide materials technology we discuss here the main factors influencing the crystal quality.

5.4.1 Raw Material Purity

As a rule, the criteria on the raw material purity are the first being discussed at the initial stage of the scintillator production technique development. Undoubtedly, the striving for the best purity of the initial components is important, but it does not necessarily guarantee, however, the final material quality. The raw material cost should also be taken into account. An improvement in purity by a factor of 10 (99.999% to 99.9999% for instance) corresponds to an increase in the cost by one order of magnitude.

As was shown in Chap. 5 some impurities and imperfections present in a crystal at the level of a few ppm may influence the optical quality, decrease the radiation hardness, and increase the afterglow. Therefore, the criteria for uncontrolled impurities and for an appropriate raw material specification have to be considered for each crystal specifically. The initial raw material requirements for optimal PWO crystals growth are mentioned in Sect. 5.2.5.

5.4.2 Raw Material Treatment and Preparation for the Crystal Growth

Interesting examples of raw material preparation methods concern fluoride scintillation crystals. Such materials are not only influenced by the initial component purity but also by the possible occurrence of salt hydrolysis during the storage, the preparation for crystal growth and single crystal growth itself. It is therefore necessary to purify the raw material and to control the atmosphere at the pregrowing and growing stages.

The fluoride hydrolysis of alkaline and alkali-metal (M) elements under the influence of atmosphere and adsorbed moisture can be described by the reaction

$$2\mathrm{MeF} + \mathrm{H_2O} \rightarrow \mathrm{Me_2O} + 2\mathrm{HF}\ ,$$
$$\mathrm{MeF_2} + \mathrm{H_2O} \rightarrow \mathrm{MeO} + 2\mathrm{HF}\ .$$

The resulting oxides are not isomorphic with the basic material and their traces in the crystal generally decrease its transparency and increase its sensitivity to radiation. Moreover they are often a source of strong afterglow [33].

Another example is the family of the most commonly used halide scintillators based on alkali-metal iodides. This material is highly hygroscopic and is subject to different reactions with atmosphere components. At least 17 chemical reactions describing different interactions with water, oxygen, carbonates, etc. have been analyzed so far [2]. Some examples of such reaction were referred in Chap. 5.

The products of these reactions lead to the contamination of the scintillation crystals both at the initial raw material synthesis stage and during the single crystal growth process. Therefore the methods of preparing the raw materials play a very important role and constitute a large part of the producer's "know-how."

5.4.3 Special Atmosphere for the Crystal Growth

Pregrowth raw material treatment is however not a sufficient condition to guarantee the optimal scintillator performance. Therefore these crystals are always grown in very specific atmospheric conditions. The atmosphere includes various fluorinating agents providing different recovery reactions, for example,

$$\begin{aligned}
\mathrm{MeO} + 2\mathrm{HF} &\rightarrow \mathrm{MeF_2} + \mathrm{H_2O}\ , \\
2\mathrm{MeO} + \mathrm{C_2F_4} &\rightarrow 2\mathrm{MeF_2} + 2\mathrm{CO}\ , \\
2\mathrm{MeO} + \mathrm{CF_4} &\rightarrow 2\mathrm{MeF_2} + \mathrm{CO_2}\ , \\
2\mathrm{MeO} + 2\mathrm{F_2} &\rightarrow 2\mathrm{MeF_2} + \mathrm{O_2}\ , \\
\mathrm{MeO} + \mathrm{CF_4} &\rightarrow \mathrm{MeF_2} + \mathrm{CO} + \mathrm{F_2}\ , \\
\mathrm{MeO} + \mathrm{F_2} + \mathrm{CO} &\rightarrow \mathrm{MeF_2} + \mathrm{CO_2}\ .
\end{aligned}$$

As a result, oxides are partly decomposed, and the remaining gas components are removed from the growing furnace by pump-out.

Recently, this problem has been highlighted by the growing interest for complex fluoride compounds such as $\mathrm{LiBaF_3}$:Ce, $\mathrm{LiCaAlF_6}$:Ce, $\mathrm{LiYF_4}$:Ce. Water and air components are the main contaminants for all these crystals [34]. Oxygen is commonly produced from OH ions and is an impurity. When such impurities are present, they can form oxy-complex such as $\mathrm{Me(OH)_2}$ [35]. Practical recommendations to eliminate or to at least minimize these impurities include for instance the raw material treatment for several hours in $\mathrm{CF_4}$ atmosphere [36]:

$$\mathrm{CF_4} + 2\mathrm{H_2O} \rightarrow 4\mathrm{HF} + \mathrm{CO_2}\ .$$

The use of $\mathrm{CF_4}$ atmosphere has a double effect on the purification. First, this is the way to eliminate the moisture even in trace quantities. Second, the slight enrichment in HF allows the reaction with $\mathrm{M(OH^-)}$ and $(\mathrm{MO^{2-}})$ complexes present in the melt.

In the case of industrial large-size crystal growth, reactive atmosphere treatment is possible at the stage of preliminary melt preparation (see [17]). Then the melt is supplied to a conical crucible located directly in the growth chamber, where the ingress of oxygen-containing components into the growing crystal is minimized by the choice of the gas atmosphere.

5.4.4 Additional Melt Purification

It must be noted that the melt treatment can also be efficient for single crystal purification. For example, PbF_2 doping is used for the CaF_2 single crystal growth. In this case, during lead fluoride smelting (temperature 1,097 K which is lower than the temperature of calcium fluoride smelting 1,673 K), its melt reacts with calcium oxide:

$$PbF_2 + CaO \rightarrow CaF_2 + PbO \uparrow$$

resulting in volatile lead oxide formation. Thus it is possible by this way to improve the optical transparency of the material, widely used for transparent UV windows.

5.4.5 Nonstoichiometry

Another group of structure imperfections radically influencing the single crystal scintillation characteristics is connected to the presence of nonstoichiometric defects in the crystal. This is typical for halide and oxide multicomponent scintillators.

The difference in the vapor pressure of the various components leads to a progressive deviation of the stoichiometry of the melt during the growth process. A compensation for the more volatile substance needs therefore to be applied for such crystals. For the $LiYF_4$:Ce crystal for instance the initial ratio has to be 50.5% LiF : 49.5% YF_3 [37]; for $LiBaF_3$:Ce this ratio needs to be even higher 57% LiF : 43% BaF_2 [38]. In typical oxide scintillators, $Bi_4Si_3O_{12}$ for example, an extra 1–5% of Bi_2O_3 is usually used [29,39]. Nonstoichiometry is the main reason for the radiation damage level increase. It is not so easy in practice to check the crystal stoichiometry. That is why this is usually done indirectly through the measurement of the radiation hardness as it is illustrated for BGO in [39].

5.5 Light Collection

Once a scintillating crystal with properties satisfying the user's requirements has been grown, there is still a problem of designing the detector itself in such a way as to ensure the detection of the maximum number of photons. In most applications the fraction of the photons produced in the crystal converting in

the photodetector (photomultiplier, PIN diode, avalanche photodiode) can be as low as 25–30%. The light collection optimization is therefore an important part of the scintillator detector optimization.

The number of photons extracted from a scintillator is given by

$$\eta = \alpha Y \tag{5.14}$$

where α is the light collection coefficient and Y is the yield of scintillation.

Once the crystal has been optimized with the best optical transparency in the spectral range of the scintillation light the light collection efficiency is mainly determined by the number of internal reflections of the photons inside the crystal and by the coupling interface between the crystal and the photodetector. The important parameters are

- the form and dimensions of the scintillation crystal,
- the specific features of the crystal surface treatment,
- the reflecting materials, and
- the adhesive bond "scintillator–photoreceiver."

Since the number of different types of material and surface treatment is very large it is impossible to determine a priori the optimal combination of parameters.

The theory and practice of scintillation detector engineering show that the light collection optimization is very user dependent and has to be made on a case by case basis.

Ultimately a good light collection scheme should answer two problems:

- maximize the number of photons extracted from the scintillator and
- keep a good linearity of the response as a function of the incident energy deposited in the scintillator wherever the conversion took place.

In fact the problem of light collection was already formulated long time ago [40, 41]. It was initially solved by the use of integrating spheres [40].

5.5.1 Simulations

The peculiarity of the light collection is the fact that the multiple reflections on the crystal surfaces influence the angular distribution of the reflected light as a function of the surface treatment (mainly its roughness). If in general the profile of reflection (indicatrix) has, as a rule, a pronounced maximum for a reflection angle equal to the angle of the light incidence, the features of this profile are determined by the material and by its surface treatment. The efficiency of the transfer as a function of the incident angle is also very complex. However, some approximation can be made. In particular in [40, 42, 43] the calculation of light transfer with a diffuse reflector was carried out in the so-called cosine approximation. In this case the reflection indicatrix is described by the equation

$$\Psi(\theta) = \pi^{-1} \cos\theta \, . \tag{5.15}$$

There are also some other known approximations and algorithms for light collection simulation by analytical methods.

In the recent years calculations of light collection and light propagation by statistical methods (Monte Carlo technique) [42–45] have become more and more reliable. The trajectories of all the photons produced in the scintillator bulk are calculated. Monte Carlo techniques consider the random character of the light diffusion process and in particular the differences in crystal surface treatment and in the specificity of the reflecting coating.

However, statistical methods are not free from some drawbacks, such as the poor modelization of certain surface states leading to a rather wide spread of some results and the difficulty to introduce the specific structure of the light diffusion indicatrix to simplify the algorithm and to minimize the calculation time which is still very long. However, computer development and increased calculation speed allow Monte Carlo techniques to gradually take over other approaches for light collection calculations. Moreover, the existing standard programs of DETEC type convert a scientific problem into a purely technical task [46].

In practice the critical point of these methods lies on the accuracy to simulate the behavior of the reflecting surface. In general two extreme cases are considered. In the first one the light collection is considered for a scintillator with mirror-like reflecting surfaces. This is also the simplest type of surface treatment and it is easily reproducible. In the case of scintillators with a regular geometrical form and without considering the light absorption in the crystal bulk, the value α is determined by the relationship [40]

$$\alpha_{a0} = \frac{1}{2}(1 - \cos\theta_1) = \frac{1}{2}\left(1 - \sqrt{1 - \frac{n_1^2}{n_2^2}}\right) \, , \tag{5.16}$$

where n is the refraction index of the crystal.

As follows from the equation a fraction of the light cannot escape the detector [43, 47, 48] which obviously limits the light collection efficiency. In order to improve this situation the geometry of the detector or the surface state must be modified.

Calculations have been made [42, 49] demsonstrating the importance of the shape (for BGO crystals). They show that crystals with a right-angle prism shape capture more than half of the photons.

Different ways have been considered to increase the light output from a scintillator: (a) the use of a photomultiplier tube (PMT) with a window refractive index matching as closely as possible the one of the crystal, (b) the production of scattering centers inside the crystal (for example, small gas bubbles), (c) the modification of the crystal shape and, finally, the coating of the crystal with diffusion reflector [43].

The use of diffusing materials at the surfaces allows us to significantly increase the light collection on small-size detectors with an aspect ratio close to 1. Moreover, the absence of predominant directions in the light propagation helps uniformize the light output within the whole scintillator bulk.

On the other hand, numerous calculations and several applications have shown that the mirror-reflecting surfaces are more efficient for long detectors with a bad aspect ratio or when the scintillator is in the shape of a plate with the receiver mounted on a side surface.

In the recent years a lot of experimental data have been accumulated which helped better tune the simulation programs. The discordances between calculations and experiments for "standard"-shaped detectors are now minimal [44, 45]. It gives some hope to make good predictions for new and more difficult shapes of crystals.

High energy physics has spent a large effort in light collection modeling in scintillators of various shapes [45] as shown in Fig. 5.27. These calculations were verified by the experimental data in CsI(Tl) scintillators for the BELLE and BaBar [50, 51] experiments.

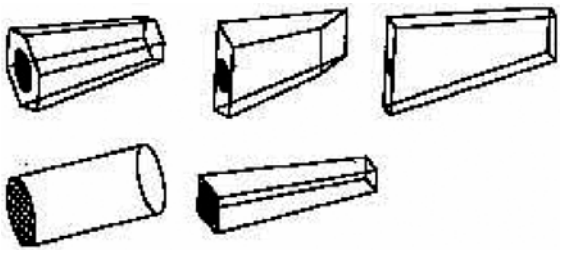

Fig. 5.27. Different shapes for HEP detectors simulated in [45]

The optimization of the light output in the 23 cm long PWO crystals for the CMS calorimeter was considered in [52]. It was shown that better light yield uniformity is achieved when one of the crystal surfaces is grinded with a specified roughness.

Scintillators for PET systems, although much smaller in size, require a precise optimization of the light collection and have been the subject of mathematical modeling [48]. Calculation by Monte Carlo technique showed that a better homogeneity of the light output can be obtained by the use of diffusion reflector with a high index of refraction and by matting the crystal face opposite to the light receiver.

The public version of the DETEC program [46] offers four different options for scintillation light collection modeling. In the METAL model, the surface is assumed to be smooth and covered by metalized coating. The PAINT model simulates diffuse reflecting surface. The POLISH and GROUND models represent surfaces that can be optically matched with other material.

Such relatively simple and available software allows us to simulate the light collection peculiarities for new scintillator configurations.

Several other simulation programs have been developed and tuned on real cases. The most complete overview of up-to-date calculation methods for light collection and typical examples of light collection simulations in scintillation detectors are presented in [44].

5.5.2 Detector Shaping

In the previous examples each crystal was considered as a single pixel which defines the coordinates of the incoming particle or γ-ray to be detected. For some applications large-size crystals are used and shaped in such a way as to provide a good uniformity of the response as well as a determination of the coordinates of the conversion point.

The idea of shaping the surface to influence the light output distribution was born 30 years ago [53]. The scheme of this light collection method is shown in Fig. 5.28.

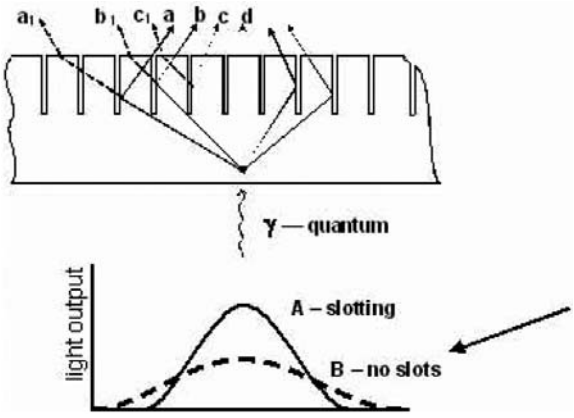

Fig. 5.28. Light collection in a slotted scintillator

The surface of the crystal is machined with slots in order to modify the conditions of light reflection at the surface. The geometry of the slots (the depth, spacing, slot filling material, etc.) is defined in order to optimize the performances for every specific application.

In [54] one-dimensional slots were cut into the entrance side of a $1''$ NaI(Tl) detector and the measurements demonstrated an improved spatial resolution. The study described in [55] showed that slots in the surface near the edge of the crystal resulted in a narrow light spread function and improved the resolution near the detector edge, thus increasing the useful area of the NaI(Tl) detector.

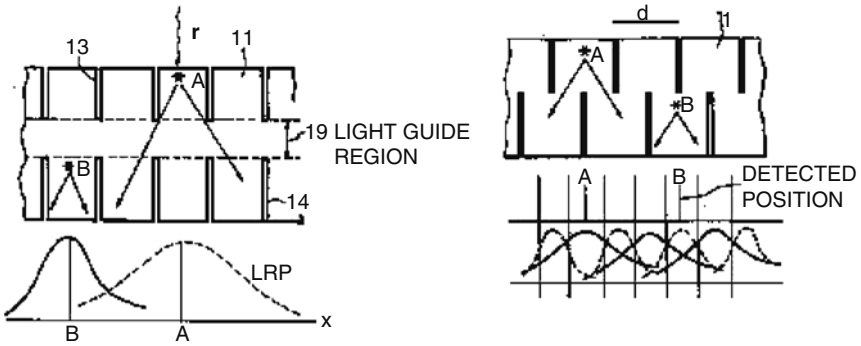

Fig. 5.29. Two surface slotting for light collection modification [57]. The bottom figures show light response functions for different scintillation flash positions

This idea found a very good application at the end of the 1990s in nuclear medicine in dual mode (SPECT-PET) systems. The StarBrite^{TM} detector from Saint Gobain with slots on the exit surface was able to produce the same light distribution in the whole energy range of the incoming γ-rays from 80 to 511 keV. Moreover, this light distribution is the same as for the conventional SPECT detectors of 9.5 mm thickness. The same readout technique as for conventional SPECT cameras is therefore directly applicable to the thick (25 mm) scintillator used for the dual mode cameras.

Figure 5.29 illustrates the influence of the slots depth and position on the light output distribution. It is interesting to notice that the slots not only collimate the light produced in the scintillator in the direction of the photomultipliers but, as a consequence of this collimation, also increase the amount of light extracted from the crystal.

Several variations of this technique have been applied. For instance, in [56] the slots were machined at the entrance surface of the scintillator. In [57] (see Fig. 5.30) the slots network was machined on both surfaces in order to give an additional information on the depth of interaction in the crystal.

The idea of the light output modification by means of surface slots has also been widely used in PET systems. The initial design based on direct coupling of the matrix detector with a PMT [58] was gradually modified by the introduction of a slotted light guide, the so-called light sharing scheme [59, 60] (see Fig. 5.30), being used in several PET systems. The individual elements have $5.8 \times 2.8\,\text{mm}^2$ cross section and 0.5 mm gap filled with reflective material.

Another example of shaping the scintillator surface for regulating the light output and improving the spatial resolution of the detector is the use of a retro-reflector. This technique can make use of a specific coating [61] or be applied directly on the crystal surface [62]. In these cases the surface of the crystal or reflector is machined to form small pyramids as in a catadioptr (therefore such type of light collection is called "retro-reflecting" [61]). The

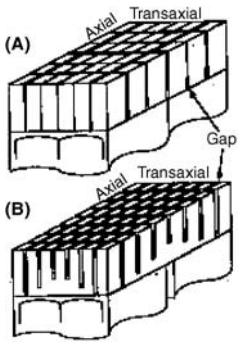

Fig. 5.30. Matrix and pseudo-discrete BGO PET block detector [59]

interest of this method is to significantly improve the light yield without decreasing the spatial resolution as would be the case with the use of a standard reflector on the back surface of the crystal (see Fig. 5.29). Such detector design allows us to reduce the influence of edge effects and to broaden the gamma camera useful field of view [62].

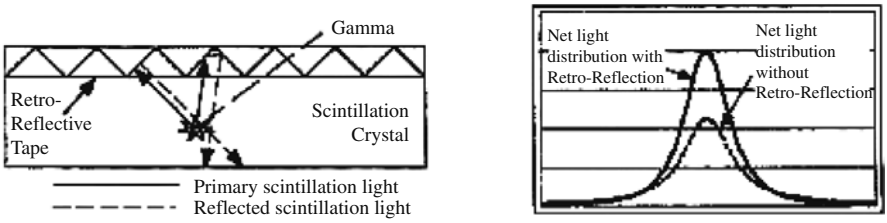

Fig. 5.31. Reflections and profiles of the light output intensity at the interface of PMT and crystal plate [61]

These examples show that the light collection optimization is one of the most important problems for scintillation detector engineering. There is a large variety of methods which have been developed for different applications on a case by case basis as the efficiency of the method is always a compromise between the choice of the scintillator material, its shape, and the technology applied for the light collection.

5.5.3 Optical Guide

The light collection optimization requires sometimes the use of a transition material between the scintillating crystal and the photodetector. In some cases the detector design does not allow us to optimally match the geometry of the scintillator with the entrances window of the photodetector. There are

in practice frequent situations of square scintillation assemblies with round cross-section PMT registration. In this case light guides are used to collect the maximum of light from the crystal and to guide it to the photodetector entrance window. Optical quartz windows are usually used as light guides particularly for near UV emitting scintillators.

Another motivation for the use of light guides is to move away the photodetector from the scintillating crystal array for position-sensitive devices. This is mandatory in the case of PMT readout in a magnetic field, or to allow a more compact design of the detection head and suppress the dead space introduced by the packaging of the photodetector.

5.5.4 Wavelength Shifters

Once the maximum number of scintillation photons have been guided to the photodetector, they still need to be converted into electrons to produce an electric signal to be processed by the readout electronics. This is the last stage of the scintillation detector optimization. In particular, the spectral sensitivity of a photodetector needs to be adjusted to the spectral range of the scintillation light. There is a large variety of PMT with different spectral sensitivities; however, a perfect matching is not always possible particularly for fast UV emitting scintillators.

One possible technique to overcome this problem is the use of wavelength shifters. It has been used to optimize the light collection in pure CsI [63]. The luminescence spectrum of such crystals is in the UV region (300–310 nm), where the sensitivity of PMT and photodiodes is very low. Usually such photodetectors have a maximum quantum efficiency in the blue or in the red spectral range. The shifters convert the UV scintillation from the crystal into visible light by the use of organic dyes (15–20 μm thick films) deposited on the crystal surface or on the photodetector entrance window. The role of the shifter is to absorb the light in the short wavelength region and to spontaneously re-emit it at a longer wavelength. The quantum efficiency of such a process may reach 90% or even more. The decay time of organic media can be very short, of the order of 1 ns, not compromising the timing performance of the scintillator. The efficiency loss resulting from this transformation can therefore be negligible as compared to the much higher losses induced by the spectral mismatch of the scintillator and the photodetector. As a result the conversion of UV luminescence into blue light can increase the overall efficiency of the detector. In [63], 10 types of scintillation dopants for polymethylphenylsioxane resins are presented to shift emissions in the 305–410 nm spectral range to the 360–550 nm range.

Figure 5.32 shows the luminescence spectrum of a CsI sample before and after coating with a wavelength shifter. Curve 3 represents the transmission of the film itself. The fast UV intrinsic luminescence of CsI (see curve 1) is absorbed by the film and shifted by about 100 nm to the region of 400 nm. Such experiments with at least five different types of wavelength shifters

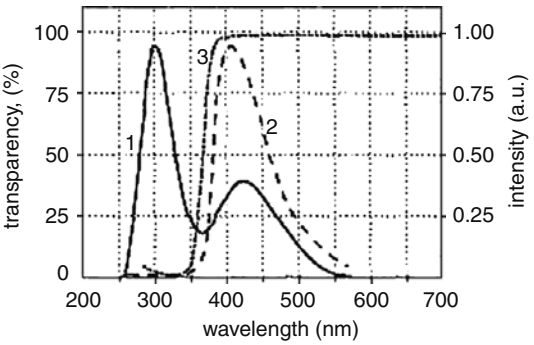

Fig. 5.32. Radioluminescence spectra of 5 mm thick, 30 mm diameter CsI sample before (*1*) and after (*2*) shifter. (*3*) Transmission spectrum of the film itself [63]

demonstrated a light output increase by a factor 1.7 to 1.8. At the same time an increase of the fast component contribution of the light from 0.6–0.7 up to 0.8–0.85 was obtained.

Such techniques are also efficient for more standard material such as CsI(Tl), in spite of, it would seem, quite well coincidence of luminescence spectrum and spectral sensitivity Si-photodiodes. The luminescence of CsI(Tl) consists of two main bands: the first one is complex and consists of several overlapped bands at 400–440 nm related to vacancy-based luminescence [65]). The main band (more intense) is at 560 nm and is caused by the exciton localization near Tl^+ ions [64]. The ratio between these bands depends on the concentration of Tl^+ ions (the blue emission more intense for a low Tl^+ contents). The use of "blue–green" shifter film (as is shown in Fig. 5.33) allows

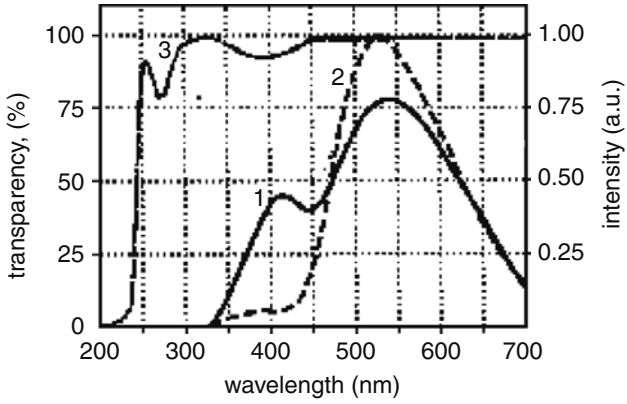

Fig. 5.33. Radioluminescence spectra of 5 mm thick, 30 mm diameter CsI sample before (*1*) and after (*2*) coating with shifter. (*3*) Transmission spectrum of the film itself. The content of Tl is 0.04 mass%

us to convert the blue emission into the green one and to increase the total light yield up to 35–40%. Such shifting is efficient for long scintillators due to a better transparency in the green than in the blue and particularly when small-size photodetectors (such as photodiodes) are used.

References

1. (a). Urusov VS (1987) Theoretical Chemistry of Crystals. Nauka, Moscow (in Russian)
   (b). Kroger FA (1964) The Chemistry of Imperfect Crystals. North-Holland, Amsterdam
2. Crystal Growth. Alkali Halides (2002) Acta, Kharkov (in Russian)
3. Kaposi O, Benese L, Zuravleva LV (1986) Determination of the thermodynamic activities by mass-spectrometry. J. Chem. Thermodyn. 18: 635–645
4. Iliasov II, Bergman AG (1966) The system Na^+, K^+, Cs^+ I^-. Inorg. Chem. B 3: 681–683 (in Russian)
5. Mahosoev MV, Alekseev FP, Lutsik VI (1978) Phase Diagram for Tungstates. Nauka, Novosibirsk (in Russian)
6. Patents of Russian Federation no 2132417, no 2164562
7. Moses WW, Derenzo SE, Fedorov A et al. (1995) $LuAlO_3$:Ce – a high density, speed scintillation for gamma detection. IEEE Trans. Nucl. Sci. 42: 275–279
8. Trower WP, Korzhik MV, Fedorov AA et al. (1996) Cerium doped luthetium-based single crystal scintillator. In: Dorenbos P, van Eijk CWE (Eds). Proc. Int. Conf. on Inorganic Scintillators and Their Applications, SCINT'95. Delft University Press, The Netherlands, pp 355–358
9. Smirnova SA, Korzhik MV (1996) Growth of crystals yttrium-aluminium perovskites with rare earth elements. In: Dorenbos P, van Eijk CWE (Eds). Proc. Int. Conf. on Inorganic Scintillators and Their Applications, SCINT'95. Delft University Press, The Netherlands, pp 495–497
10. Patent of the Russian Federation no 2233916
11. Lodis R, Parker R (1974) Crystal Growth. Rus. ed., Mir, Moscow, pp 176–183
12. von Wilke K-Th (1973) Kristallzuchtung. Wilke unter Mitarbeit von J. Bohm. VEB Deutsher Verlag der Wissenschaften, Berlin
13. Gektin AV, Zaslavsky BG (2003) Halogenide scintillators: growth and performance. In: Scheel H, Fukuda T (Eds.) Crystal Growth Technology. Wiley, New York, pp 511–536
14. US Patent 2,214,967
15. Stockbarger DC (1936) The production of large single crystals. Rev. Sci. Instrum. 7: 133–136
16. Kyropolos S, Zeits F (1926) Ein Verfahren zur Herstellung grosser Kristalls. Anorg u. allgem Chem. 154: 308–313
17. Czochralski J (1918) Ein newes Verfahren zur Messung der Kristallisatinosgeschwindigkeit der Metalle. Z. Phys. Chem. 92: 219–224
18. (a). Tanji K, Ishii M, Usuki Y et al. (1999) Crystal growth of $PbWO_4$ by the vertical Bridgman method: effect of crucible thickness and melt composition. J. Cryst. Growth 204: 505–511
    (b). Ishii M, Harada K, Hirose Y et al. (2002) Development of BSO ($Bi_4Si_3O_{12}$) crystal for radiation detector. Opt. Mater. 19: 201–212

(c). Ishii M, Kuwano Y, Asai T, Senguttuvan N et al. (2003) Growth of Cu-doped $Li_2B_4O_7$ single crystals by vertical Bridgman method and their characterization. J.Cryst. Growth 257: 169–176
19. Pfann W.G. (1966) Zone Melting. Wiley New York and London
20. Tatarchenko VA (1988) Stable Crystal Growth. Nauka, Moscow (in Russian)
21. Gektin AV (2000) Halide scintillators: present status and prospects. In: Mikhailin VV (Ed). Proc. of the Fifth Int. Conf. on Inorganic Scintillators and Their Applications, SCINT99. Moscow State University, Moscow, pp 79–88
22. U.S. Patent 4,834,832
23. U.S. Patent 4,036,595
24. Eidel'man LG, Goriletsky VI, Nemenov VA et al. (1985) Automated growing of large single controlled by melt level sensor. Cryst. Res. Technol. 20(2): 167–172
25. Zaslavsky B (1999) Automated pulling of large-diameter alkali halide scintillation single crystals from the melt. J. Cryst. Growth 200: 476–482
26. Smet F, van Enckervort WJP (1988) On the distribution of point defects in large sized bismuth germanate crystals. J. Cryst. Growth 88: 169–179
27. Borolev YuA, Ivannikova NV, Shlegel VN et al. (2001) Progress in growth of large sized BGO crystals by the low-thermal-gradient Czochralski technique. J. Cryst. Growth 229: 305–311
28. Shlegel VN, Shubin YuV, Ivannikova NV (2003) BGO crystal growth, J. Korean Cryst. Growth Cryst. Technol. 13: 1–4
29. Atroshenko L, Burachas S, Galchinetsky L et al. (1998) Scintillation crystals and radiation detectors on its base, Kiev (in Russian)
30. Gektin AV (2000) Growth and characterization of scintillation and storage materials, In: Fukuda T (Ed). Second Int. School on Crystal Growth Techn (Book of lectures), Japan, pp 304–327
31. Garmash VM, Beloglovski SYa, Lubetsi SL (2002) Industrial manufacturing of cerium-doped lutetium silicate crystals on enterprise joint-stock-company "North Crystal". Nucl Instrum. Methods Phys. Res. A 486: 106–110
32. Melcher CL, Schweitzer JS, Peterson CA et al. (1996) Crystal growth and scintilation properties of the rare earth oxyorthosilicates. In: Dorenbos P, van Eijk CWE (Eds). Proc. Int. Conf. on Inorganic Scintillators and Their Applications, SCINT'95. Delft University Press, The Netherlands, pp 309–316
33. Weller PF, Scardefield JE (1964) Doping of alkaline earth halide single crystals. J. Electorochem. Soc. 111(8): 1009–1011
34. Pastor RC (1999) Crystal growth of metal fluorides for CO_2 laser operation: I. The necessity of the RAP approach. J. Cryst. Growth 200: 510–514
35. Ranieri IM, Morato SP, Bressiani AHA et al. (2002) Growth of $LiYLuF_4$ crystals under CF_4 atmosphere. J. Alloys Compd. 344: 203–206
36. Belt R, Uhrin R (1991) Top seeded solution growth of Cr^{3+}: $LiCaAlF_6$ in HF atmosphere. J. Cryst. Growth 109: 334–339
37. Raineri I, Baldochi S, Santo A (1996) Growth of $LiYF_4$ crystals doped with holmium, erbium and thulium. J. Cryst. Growth, 166: 423–428
38. Baldochi S, Shimamura K, Nakano K et al. (1999) Growth and optical characteristics of Ce-doped and Ce:Na-codoped $BaLiF_3$ single crystals. J. Cryst. Growth 200: 521–526
39. (a) Shulgin BV, Polupanova TI, Kruzalov AV, Skorikov VM (1992) Bithmut Orthogermanate Ecaterinburg, p 170 (In Russian)

(b) Gusev VA, Kupriyanov IN, Antsygin VD et al. (2001) Features of radiation damage of BGO crystals grown by the low-thermal-gradient Czochralski technique. Nucl. Instrum. Methods Phys. Res. A 460: 457–464
40. Tsirlin YuA. (1975) Light Collection in the Scintillation Counters. Atomizdat, Moscow (in Russian)
41. Tsirlin YuA, Globus ME, Sysoeva EP (1991) Optimization of Gamma Detection in Scintillation Crystals. Energoatomizdat, Moscow (in Russian)
42. Derenzo SE, Rilers JK (1982) Monte-Carlo calculations of the optical coupling between bismuth-germanate crystals and photomultiplier Tubes. IEEE Trans. Nucl. Sci. 29: 191–194
43. Carrier C, Lecomte R (1990) Theoretical modelling of light transport in rectangular parallelepipedic scintillators. Nucl. Instrum. Methods Phys. Res. 292(3): 685–692
44. Globus ME, Grinyov BV (2001) Inorganic new and conventional scintillators. Acta, Kharkov (in Russian)
45. Gavriluk VP, Vinograd EL, Grinyov BV et al. (1997) Effect of surface conditions on the light collection in scintillation detectors. Search for optimum light collection conditions in cylindric scintillation detectors. Funct. Mater. 4: 572–583
46. Knoll GF, Knoll TF, Henderson TM (1988) Light collection in scintillation detector composites for neutron detection. IEEE Trans. Nucl. Sci. 35: 872–875
47. Carrier C, Lecomte R (1989) Trapping of fluorescent light in cylindrical scintillators. Nucl. Instrum. Methods Phys. Res. A 288(2): 622–624
48. Carrier C, Lecomte R (199) Effect of geometrical modifications and crystal shapes on light collection in ideal rectangular parallelepipedic BGO scintillators. Nucl. Instrum. Meth Phys. Res. A 294(1–2): 355–364
49. Derenzo SE (1984) Gamma-ray spectroscopy using small, cooled bismuth germinate scintillators and silicon photodiods. Nucl. Instrum. Methods Phys. Res. 219: 117–122
50. BaBar Collaboration, BaBar Technical Design Report, SLAC-R-95-457
51. Gektin AV, Gavrylyk V, Zosim D, Yankelevich V, (2000) Long length scintillators for the position sensitive radiation detection IEEE NSS/MIC Abstracts 58
52. Auffray E., Lecoq P., Schneegans M. et al. (2002) Crystal conditioning for high-energy physics detectors. Nucl. Instrum. Meth. Phys. Res. A 486: 22–34
53. Patent France 2,237,206.
54. Freifelder R, Haigh AT, Karp JS (1993) Reducing edge effects and improving position resolution in position sensitive NaI(TI) detectors. IEEE Trans. Nucl. Sci. 40: 208–213
55. Yu DC (1997) Light output distribution in slotted crystal. IEEE MIC Conf. Rec. Paper M10-24
56. Surti S, Freifelder R, Karp JS (2001) Slotted surface treatment of position-sensitive NaI(Tl) detectors to improve detectors performance. IEEE Trans. Nucl. Sci. 48: 2418–2423
57. U.S. Patent 4,831,263
58. U.S. Patent 5,091,650
59. Tornai MP, Germano G, Hoffman E (1994) Positioning and energy response of PET block detectors with different light sharing schemes. IEEE Trans. Nucl. Sci. 41: 1458–1463

60. Rogers JP, Taylor AJ, Rahimi MF et al. (1992) An improved multicrystal 2-D BGO detector for PET. IEEE Trans. Nucl. Sci. 39(4): 1063–1068
61. McElroy DP, Sung-Cheng Huang, Hoffman EJ (2002) The use of retro-reflective tape for improving spatial resolution of scintillation detectors**.** IEEE Trans Nucl Sci 49: 165–171
62. U.S. Patent 5,861,628
63. (a) Andryushenko LA, Vinograd EL, Gavriliuk VP et al. (1997) An influence of surface conditions on the scintillation properties of CsI crystals. IET 4: 19–21 (in Russian)
(b) Andryushenko LA, Kudin AM, Goriletsky VI et al. (2002) Functional possibilities of organosilicon coatings on the surface of CsI-based scintillators. Nucl. Instrum. Methods Phys. Res. A 486: 40–47
64. Zazubovich S, Karner T, Nagirnyi V et al. (1996) Exciton luminescence in Tl^{+} and Pb^{2+} doped cesium halides. In: Shreiber M (Ed). Extonic Process in Condensed Matter, Dresden University Press, pp 235–238
65. Bates CW Jr, Schneider I, Salau A et al. (1976) X-ray diffraction measurement of the Jahn–Teller distortion in $TmVO_4$. Solid State Commum. 15: 101–104